Free Vibrations of Multispan Continuous Arches

다경간 연속아치의 자유진동 해석

Lee, Byoung Koo · Oh, Sang Jin · Mo, Jeong Man · Lee, Yong
이 병 구*·오 상 진**·모 정 만**·이 용**

적 요

본 논문은 다경간 연속아치의 자유진동에 관한 연구이다. 다경간 연속아치의 고유진동수 및 진동형을 산출하기 위하여 내부지점의 지점조건에 따른 경계조건식을 유도하였다. 아치의 선형은 포물선을 택하였으며, 회전-로울러-회전, 고정-회전-고정의 지점조건을 갖는 2경간 연속아치에 대한 수치해석 결과를 제시하였다. Runge-Kutta method를 이용하여 지배방정식을 수치적분하였으며, 고유치를 찾기 위해서는 행렬값탐사법을 이용하였다. 실제 수치해석예에서는 회전관성이 고유진동수에 미치는 영향을 고찰하였으며, 무차원 고유진동수와 아치높이 지간길이비 및 세장비 사이의 관계를 분석하였다. 또한 실험을 통하여 이론적인 해석결과를 검증하였다.

I. Introduction

Since arches are basic structural forms, their dynamics and especially free vibrations have been studied extensively. The following references and their citations include the governing equations and significant historical literature on the in-plane vibrations of linearly elastic arches of various geometries and end constraints. Such studies were critically reviewed by Laura and Maurizi[7]. Background material for the current study was summarized by Lee and Wilson[9].

Briefly, such works included studies of circular arches with predictions of higher flexural frequencies by Wung[19], Wolf[18], Velet-

* Professor, Wonkwang University
** Graduate student, Wonkwang University

Key words : arch, boundary condition, dynamics, experiments, free vibration, mode shape, multispan, natural frequency, Regula-Falsi method, Runge-Kutta method, rotary inertia

sos et al.[14], and Austin and Veletsos[1]; studies of non-circular arches with predictions of the lowest frequency in flexure by Romanelli and Laura[12], and in extension by Lee and Wilson[9], Wang[15], and Wang and Moore[16]; studies of arches with variable cross-section with predictions of higher flexural frequencies by Sakiyama[13] and Wilson, Lee and Oh [17]. Experimental studies to validate predicted arch frequencies and mode shapes are rare, although recent such studies on selected arches were reported by Wilson, Lee and Oh [17], Perkins[11], and Lee and Wilson[10].

The main purpose of the present paper is to investigate the free vibrations of multispan continuous arches, both theoretically and experimentally. In the most previous works on arch vibrations, only the arches with simple span were considered. The arches with multiple spans are reported for the first time in this study. The boundary conditions of intermediate supports are derived for such arches. The numerical results are presented for parabolic arches with the hinged-roller-hinged and clamped-hinged-clamped end constraints. The computed results are then validated with experimental results measured from the laboratory-scale models of arches.

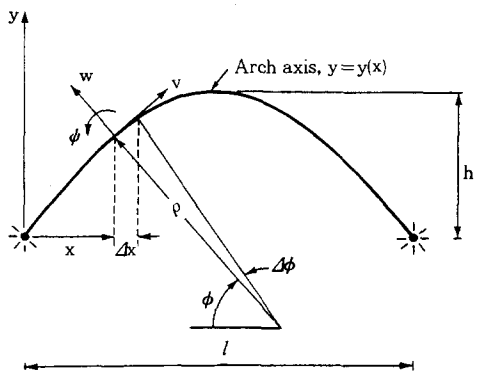

Fig. 1. Arch geometry

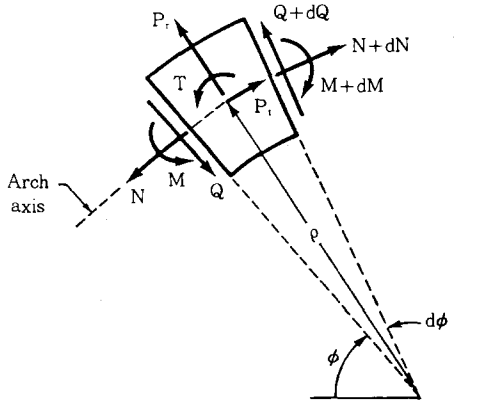

Fig. 2. Loads on an arch element

II. Differential equations

The geometry of the uniform, symmetric arch with simple span is defined in Fig. 1. Its span length, rise, and shape of the middle surface are l, h, and y(x), respectively. Its radius of curvature ρ, a function of the coordinate x, has an inclination ϕ with the x-axis. Also shown in Fig. 1 are the positive directions of radial and tangential displacements, w and v, and positive direction of rotation ϕ of cross-section.

A small element of the arch shown in Fig. 2 defines the positive directions for the axial force N, the shear force Q, the bending moment M, the radial inertia force P_r, the tangential inertia force P_t, and the rotary inertia couple T. With the inertia forces and the inertia couple treated as equivalent static quantities, the three equations for "dynamic equilibrium" of the element are

$$dN/d\phi + Q + \rho P_t = 0 \quad \cdots\cdots (1)$$
$$dQ/d\phi - N + \rho P_r = 0 \quad \cdots\cdots (2)$$
$$dM/d\phi - \rho Q - \rho T = 0 \quad \cdots\cdots (3)$$

The equations that relate N, M and ϕ to the displacements w and v account for axial deformation due to N. These equations, given by Borg and Gennaro[2], are

$$N = EA\rho^{-1}[(v' + w) + r^2\rho^{-2}(w'' + w)] \cdots (4)$$

$$M=-EAr^2\rho^{-2}(w''+w) \quad \cdots\cdots(5)$$
$$\phi=\rho^{-1}(w'-v) \quad \cdots\cdots(6)$$

where $(')=d/d\phi$, E is the Young's modulus, A is the cross-sectional area, and r is the radius of gyration of cross-section.

The arch is assumed to be in harmonic motion[6], or each co-ordinate is proportional to $\sin(\omega t)$, where ω is the angular frequency and t is time. The inertia loadings are then

$$P_r=\gamma\omega^2 w \quad \cdots\cdots(7)$$
$$P_t=\gamma\omega^2 v \quad \cdots\cdots(8)$$
$$T=\gamma\omega^2 r^2\phi = \gamma\omega^2 r^2\rho^{-1}(w'-v) \quad \cdots\cdots(9)$$

where γ is mass per unit length.

When equations (4) and (5) are differentiated once, the results are

$$dN/d\phi=EA\rho^{-1}[(v''+w')+r^2\rho^{-2}(w'''+w')-\rho'\rho^{-1}(v'+w)-3r^2\rho'\rho^{-3}(w''+w)] \quad \cdots\cdots(10)$$
$$dM/d\phi=-EAr^2\rho^{-2}[(w'''+w')-2\rho'\rho^{-1}(w''+w)] \quad \cdots\cdots(11)$$

When equations (9) and (11) are substituted into equation (3), then

$$Q=\rho^{-1}dM/d\phi-RT = -EAr^2\rho^{-3}[(w'''+w')-2\rho'\rho^{-1}(w''+w)]-R\gamma\omega^2 r^2\rho^{-1}(w'-v) \quad \cdots\cdots(12)$$

where the index R=1 if the rotary inertia couple is included and R=0 if T is excluded.

The following equation is obtained by differentiating equation (12):

$$dQ/d\phi=-EAr^2\rho^{-3}[(w''''+w'')-5\rho'\rho^{-1}(w'''+w')+2\rho^{-1}(4\rho'^2\rho^{-1}-\rho'')(w''+w)]-R\gamma\omega^2 r^2\rho^{-1}[(w''-v')-\rho'\rho^{-1}(w'-v)] \quad \cdots\cdots(13)$$

To facilitate the numerical studies, the following non-dimensional system variables are defined. The first is the frequency parameter,

$$C_i=\omega_i l^2 r^{-1}(\gamma/EA)^{1/2}, i=1,2,3,\cdots \quad (14)$$

which is written in terms of ith frequency $\omega=\omega_i$, i=1,2,3,... The arch rise to span length ratio f and the slenderness ratio s are, respectively,

$$f=h/l \quad \cdots\cdots(15)$$
$$s=l/r \quad \cdots\cdots(16)$$

The co-ordinates, the displacements and the radius of curvature are normalized by the span length l:

$$\xi=x/l \quad \cdots\cdots(17)$$
$$\eta=y/l \quad \cdots\cdots(18)$$
$$\delta=w/l \quad \cdots\cdots(19)$$
$$\lambda=v/l \quad \cdots\cdots(20)$$
$$e=\rho/l \quad \cdots\cdots(21)$$

When equations (13), (4), and (7) are substituted into equation (2) and equations (14)-(21) are used, the result is

$$\delta''''=a_1\delta'''+(a_2+Ra_3s^{-4}C_i^2)\delta''+(a_1-Ra_4s^{-4}C_i^2)\delta'+(a_5+a_6s^{-4}C_i^2)\delta+(1-Rs^{-4}C_i^2)a_3\lambda'+Ra_4s^{-4}C_i^2\lambda \quad \cdots\cdots(22)$$

When equations (10), (12) and (8) are substituted into equation (1) and equations (14)-(21) are used, the result is

$$\lambda''=a_7\delta''+(Rs^{-4}C_i^2-1)\delta'+a_8\delta+a_9\lambda'+(a_3-R)s^{-4}C_i^2\lambda \quad \cdots\cdots(23)$$

The coefficients in the last two equations are

$$a_1=5e'e^{-1} \quad \cdots\cdots(24)$$
$$a_2=2e''e^{-1}-8e'^2e^{-2}-2 \quad \cdots\cdots(25)$$
$$a_3=-s^2e^2 \quad \cdots\cdots(26)$$
$$a_4=-s^2ee' \quad \cdots\cdots(27)$$
$$a_5=2e''e^{-1}-8e'^2e^{-2}-s^2e^2-1 \quad \cdots\cdots(28)$$
$$a_6=s^4e^4 \quad \cdots\cdots(29)$$
$$a_7=e's^{-2}e^{-3} \quad \cdots\cdots(30)$$
$$a_8=e'e^{-1}(1+s^{-2}e^{-2}) \quad \cdots\cdots(31)$$
$$a_9=e'e^{-1} \quad \cdots\cdots(32)$$

The coefficients defined by equations (24)-(32) are computed as follows. Cast the given arch shape y=y(x) in non-dimensional form using equation (15), (17) and (18). This leads to

$$\eta=\eta(\xi) \quad \cdots\cdots(33)$$

from which the slenderness ratio s is identified. By definition

$$\phi=\pi/2-\tan^{-1}(d\eta/d\xi) \quad \cdots\cdots(34)$$
$$e^{-1}=d^2\eta/d\xi^2[1+(d\eta/d\xi)^2]^{-3/2} \quad \cdots\cdots(35)$$

Both ϕ and e are computed from derivatives of equations (33) and are expressed as functions of the single variable ξ. Then e′ and e" are calculated from the derivatives of equations (34) and (35) by using

$$e'=de/d\xi\cdot d\xi/d\phi \quad \cdots\cdots(36)$$
$$e''=de'/d\xi\cdot d\xi/d\phi \quad \cdots\cdots(37)$$

Now the calculation procedure of the coefficients defined by equations (24)-(32) is illustrated for the parabolic arch using equations (33)-(37). The general equation for the parabolic arch of span length l and rise h(see Fig. 1) is

$$y=-4hl^{-2}x(x-l),\ 0\le x\le l \quad \cdots\cdots(38)$$

With equations (15), (17) and (18), the non-dimensional form of equation (38) becomes

$$\eta=-4f\xi(\xi-1),\ 0\le\xi\le 1 \quad \cdots\cdots(39)$$

With equation (39), the following equations are calculated from equations (33)-(37):

$$\phi=\pi/2-\tan^{-1}[-4f(2\xi-1)] \quad \cdots\cdots(40)$$
$$e=0.125f[1+16f^2(2\xi-1)^2]^{3/2} \quad \cdots\cdots(41)$$
$$e'=1.5(2\xi-1)[1+16f^2(2\xi-1)^2]^{3/2} \quad \cdots\cdots(42)$$
$$e''=0.375f[1+64f^2(2\xi-1)^2][1+16f^2(2\xi-1)^2]^{3/2} \quad \cdots\cdots(43)$$

Thus, the coefficient a_1 through a_9 can be calculated by the single variable ξ.

In order to derive the intermediate boundary conditions, the bending moment M, axial force N and shear force Q are normalized as follows.

$$m=Ml/EI=-e^{-2}(\delta''+\delta) \quad \cdots\cdots(44)$$
$$n=Nl^2/EI=s^2e^{-1}[(\lambda'+\delta)+s^{-2}e^{-2}(\delta''+\delta)] \quad \cdots(45)$$
$$q=Ql^2/EI=-e^{-3}[(\delta'''+\delta')-2e'e^{-1}(\delta''+\delta)]-RC_i^2s^{-2}e^{-1}(\delta'-\lambda) \quad \cdots\cdots(46)$$

III. Boundary conditions

Now the multispan continuous arches are introduced for deriving the boundary conditions. For examples, the two symmetric arches with two and three spans, respectively, are shown in Fig. 3, in which the H, C and R are depicted as the hinged, clamped and roller supports, respectively. As shown in this figure, the two far ends of arches are supported by either both hinged or both clamped constraints and the intermediate supports are either roller or hinged supports.

The first boundary conditions are for the far ends. The boundary conditions of hinged ends($\xi=0$ for first span or $\xi=1$ for last span) are

$$\lambda=0 \quad \cdots\cdots(47)$$
$$\delta=0 \quad \cdots\cdots(48)$$
$$\delta''=0 \quad \cdots\cdots(49)$$

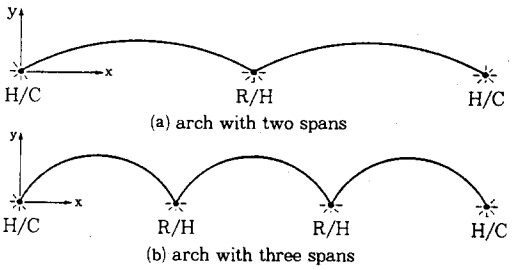

Fig. 3. Examples of multispan continuous arch

where the last condition assures that the non-dimensional bending moment m given by equation (44) is zero.

The boundary conditions of clamped ends ($\xi=0$ for first span or $\xi=1$ for last span) are

$$\lambda = 0 \quad \cdots\cdots(50)$$
$$\delta = 0 \quad \cdots\cdots(51)$$
$$\delta' = 0 \quad \cdots\cdots(52)$$

where the last condition assures that the end rotation ψ given by equation (6) is zero.

The second boundary conditions are for the intermediate supports which are either roller or hinged supports. The undeformed and deformed roller supports are shown in Fig. 4, in which β is the slope angle at the roller support. The three non-dimensional m, n and q of the left span at $\xi=1$ are equal to those of the right span at $\xi=0$, respectively, as shown in Fig. 4. Thus, the following equations are obtained by equations (44)-(46).

$$e^{-2}(\delta''_R+\delta_R)+m_L=0 \quad \cdots\cdots(53)$$
$$s^2e^{-1}[(\lambda'_R+\delta_R)+s^{-2}e^{-2}(\delta''_R+\delta_R)]$$
$$-n_L=0 \quad \cdots\cdots(54)$$
$$e^{-3}[(\delta'''_R+\delta'_R)-2e'e^{-1}(\delta''_R+\delta_R)]$$
$$+RC_i^2s^{-2}e^{-1}(\delta'_R-\lambda_R)+q_L=0 \quad \cdots\cdots(55)$$

in which the subscripts R and L mean the left and right span, respectively.

The three deformations δ, λ and ψ can be used as the boundary conditions. The rotation of cross section ψ of left span at $\xi=1$ and that of right span at $\xi=0$ are equal to each other. Thus, this gives the following equation.

$$e^{-1}(\delta'_R-\lambda_R)-\psi_L=0 \quad \cdots\cdots(56)$$

At the roller supports, the horizontal and vertical components of the displacement between δ and λ of left span are equal to those of right span and this gives the following equations.

$$\delta_R\cos\alpha-\lambda_R\cos\beta=-(\delta_L\cos\alpha+\lambda_L\cos\beta) \quad \cdots(57)$$
$$\delta_R\sin\alpha+\lambda_R\sin\beta=\delta_L\sin\alpha-\lambda_L\sin\beta \quad \cdots\cdots(58)$$

where α is $\pi/2-\beta$.

Above equations (53)-(58) are the boundary conditions for the intermediate roller supports.

At the intermediate hinged supports, the equations (53)-(56) are available and no displacement is allowable so that the following equations are obtained.

$$\lambda_L=\lambda_R=0 \quad \cdots\cdots(59)$$
$$\delta_L=\delta_R=0 \quad \cdots\cdots(60)$$

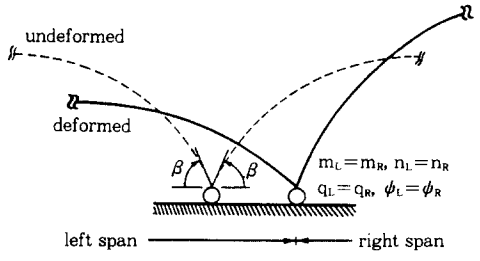

Fig. 4. Intermediate roller support

IV. Numerical methods

A FORTRAN computer program was written to calculate natural frequencies and mode shapes. The numerical methods similar to those described by Lee and Wilson[9], Wilson, Lee and Oh[17] and Lee, Oh and Mo[8] were used to solve the differential equations (22) and (23) subject to the boundary conditions of far ends of equations (47)-(49) or (50)-(52) and that of intermediate supports of equations (53)-(58). For the sake of completeness, this numerical procedure is summarized as follows.

1. Specify R(=0 or 1), the arch geometry (f, s), the set of three homogeneous boundary constraints which are either equations (47)-(49) or (50)-(52), and intermediate supports which

are either rollers or hinged supports.

2. Consider the sixth order system, equations (28) and (29), as three initial value problems whose initial values are the three homogeneous boundary constraints $\xi=0$, as chosen in step 1. Then assume a trial frequency parameter C_i in which the first trial value is zero.

3. Using the Runge-Kutta method[3], integrate equations (28) and (29) from $\xi=0$ to $\xi=1$ for the first span. Perform three separate integrations, one for each of the three chosen end constraints.

4. Calculate the initial values δ_R''', δ_R'', δ_R', δ_R, λ_R', and λ_R for second span using equations (53)-(58) and integrate equations (28) and (29) from $\xi=0$ to $\xi=1$.

5. Repeat step 4 for third, fourth, ..., and last span.

6. From the Runge-Kutta solution, evaluate at $\xi=1$ of the last span, the determinant D of the coefficient matrix for the chosen set of three homogeneous boundary conditions. If $D=0$, then the trial value of C_i is an eigenvalue. If $D\neq 0$, then increment C_i and repeat step 3-6.

7. Note the sign of D in each iteration of processing step 3-6. If D changes sign between two consecutive trials, then the eigenvalue lies between these last two trial values of C_i.

8. Use the Regula-Falsi method[5] to compute the advanced trial C_i based on its two previous values.

9. Terminate the calculations and print the value of C_i and the corresponding mode shapes when the convergence criteria are met.

The step size used in the Runge-Kutta method was calculated from equation (34), or

$$\Delta\phi=\tan^{-1}(d\eta/d\xi)_{\xi}-\tan^{-1}(d\eta/d\xi)_{\xi+\Delta\xi} \quad \cdots(61)$$

where it recall that $d\eta/d\xi$ is a known function of ξ for arch geometry. $\Delta\phi$ and $\Delta x(=l\Delta x)$ are depicted in Fig. 1.

V. Numerical results and discussion

For the numerical studies herein, suitable convergence of solutions were obtained for an increment of $\Delta\xi=1/100$. The convergence criterion was that C_i solutions obtained with more crude increment of 1/30 agreed with those obtained with the 1/100 increment to within three significant figures. The numerical results in which the lowest few natural frequencies and corresponding mode shapes were calculated are now discussed.

Selected studies were made to show the effect of rotary inertia on the three lowest frequencies of hinged-roller-hinged with $f=0.1$, $s=10.\sim100.$ and clamped-hinged-clamped arches with $f=0.3$ and $s=10.\sim100.$ Typical results are shown in Table 1, in which the

Table-1. Effects of rotary inertia on natural frequency

Geometry of arch	s	R	Frequency parameter, C_i		
			i=1	i=2	i=3
hinged-roller-hinged	10	0	9.361	16.18	18.67
and f=0.1		1	8.915	15.71	16.23
	20	0	9.173	20.21	30.21
		1	9.056	19.44	30.03
	30	0	9.121	24.79	36.55
		1	9.076	24.32	34.98
	50	0	9.106	35.64	36.63
		1	9.085	35.39	36.04
	100	0	9.107	36.34	45.68
		1	9.089	36.30	45.51
clamped-hinged	10	0	17.14	19.90	24.87
-clamped and f=0.3		1	16.67	19.53	22.19
	20	0	26.40	32.48	32.86
		1	25.95	32.17	32.30
	30	0	27.84	35.43	47.10
		1	27.56	35.30	45.76
	50	0	28.25	36.35	65.31
		1	28.13	36.00	65.17
	100	0	28.37	36.36	67.13
		1	28.34	36.26	66.78

lowest three natural frequencies were calculated. From these and other results, the following conclusions were reached. (1) Frequencies(or C_i values) are always somewhat lower with rotary inertia (R=1) than without (R=0); such a result is to be expected. (2) This frequency depression is accentuated as the slenderness ratio s decreases from 100 to 10; and also as i increases at constant s. (3) In practical designs, s is generally greater than 20, for which rotary inertia depresses the frequencies: by 1% or less for i=1 and by 5% for i=2,3.

The numerical results of Figs. 5-9 do, how-

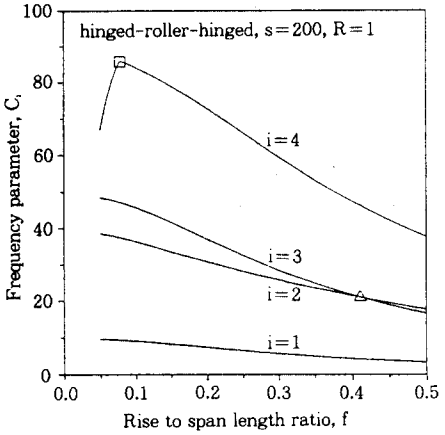

Fig. 5. C_i-f curve(HRH)

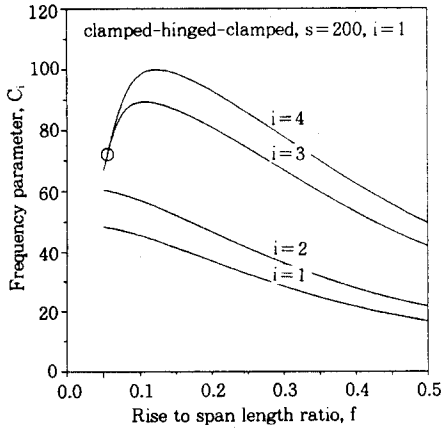

Fig. 6. C_i-f curve(CHC)

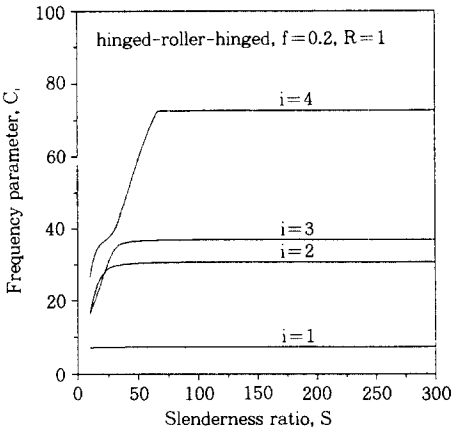

Fig. 7. C_i-s curve(HRH)

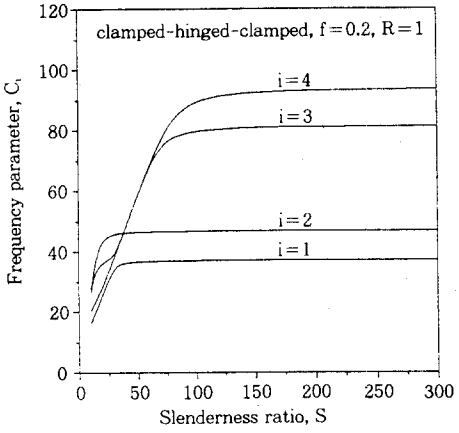

Fig. 8. C_i-s curve(CHC)

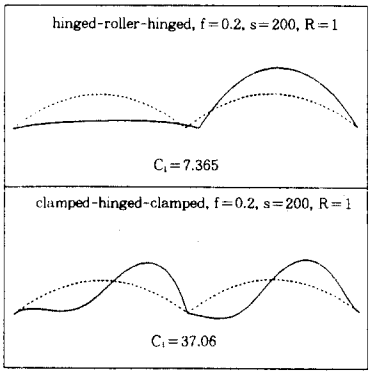

Fig. 9. Typical example of first mode shapes

ever, include the effects of rotary inertia, in which the lowest four natural frequencies were calculated.

It is shown in Fig. 5, for which hinged-roller-hinged arch with s=200 and R=1, that the frequency parameters C_i(i=1,2,3,4) decrease as the rise to span length ratio f is increased, generally. Further, it is observed for these two span continuous arch configurations that two modes can exist at a single frequency, a phenomena that was previously observed only for one span arch configurations by Lee and Wilson[9]. For these arches, the second and third modes have the same frequency at $C_2=C_3=20.86$ and f=0.412 (marked △). And it is clear that the fourth and fifth(not shown) modes have the same frequency since the curve of i=4 have an inflection point at marked □. Also this figure exhibits the common feature that as the rise to span length ratio f is increased, the frequency parameters all approach common values, may be zero, because the arch is more flexible in the bending vibration in larger f values. It is shown in Fig 6, for which clamped-hinged-clamped arch with s=200 and R=1, that the third and fourth modes have the same frequency at $C_3=C_4=70.37$ and f=0.0535 (marked ○) as discussed in Fig. 5.

The Figs. 7 and 8 show the effects of the slenderness ratio s on frequency parameters C_i of the hinged-roller-hinged and clamped-hinged-clamped arches, respectively, with f =0.2 and R=1. In these figures, it is found that the frequency parameters C_i increase, and in most cases approach a horizontal asymptote, as the slenderness ratio s is increased. Also, the phenomena that two modes can exist at a single frequency are shown in these figures.

The typical examples of the first mode shapes of hinged-roller-hinged and clamped-hinged-clamped arches with f=0.2, s=200 and R=1, in which both mode shapes are anti-symmetric modes. Since the arches presented in this study are symmetric, the mode shapes are either symmetric or anti-symmetric modes. Even though not shown in this paper, the symmetric mode shapes were existed in the numerical examples of this study.

VI. Experimental results and discussion

Two laboratory-scale parabolic arches, a hinged-roller-hinged and a clamped-hinged-clamped configuration, were designed and tested to determine their lowest few natural frequencies. The main purpose of these experiments was to validate the proposed mathematical model and typical numerical solutions predicted herein.

The experimental models were bent from steel bar stock to the parabolic shape with (x,y) co-ordinates described by equation (38). The geometric arch parameters of one span were: l=30 cm, h=7.5 cm with a width and thickness for rectangular cross-section of 3 cm and 0.2 cm, respectively(A=0.6 cm^2, r= 0.0577 cm). The corresponding non-dimensional arch parameters were thus f=h/l=0. 25 and s=l/r=520. The frequencies C_i are calculated using the material properties of steel: a Young's modulus E of 2.0×10^7 N/cm^2 and mass density of 7.85×10^{-5} N-sec^2/cm^4, for which γ, the mass per unit length of arc, is 4.71×10^{-5} N-sec^2/cm^2. The predicted frequencies for the experimental arches are thus $f_i=32.4C_i$ rad/s=$5.15C_i$ Hz from equation (14), and these numerical values are listed in Table 2.

The experimental setup is shown in Fig. 10. The procedures for measuring frequencies and the methods for reducing data[4] are summarized. At each support, the arch was either hinged or clamped or roller to a steel connection attached to a concrete block. Each block "floated" on a soft rubber pad to achieve vibration isolation. In these experi-

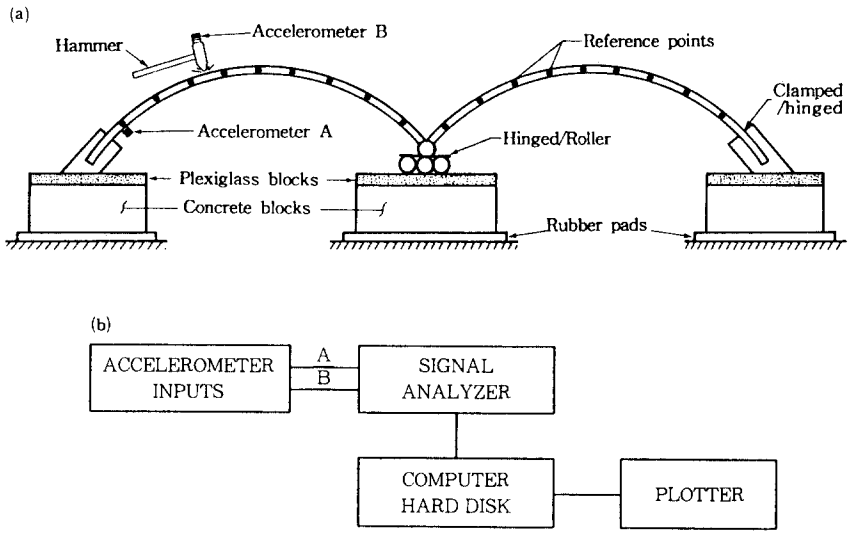

Fig. 10. Schematic drawings of : (a) typical experimental setup : (b) modal analysis system

Table-2. Comparison of computed and measured results(f=0.25, s=520)

End constraint	i	Theory		Experiment	% Deviation
		C_i	f_i(Hz)	f_i(Hz)	
clamped	1	32.56	167.7	157.	-6.4
-hinged	2	41.42	213.3	194.	-9.0
-clamped	3	74.27	382.5	347.	-9.3
	4	85.99	442.8	380.	-14.2
hinged-roller	1	6.465	33.29	30.6	-8.1
-hinged	2	28.17	145.1	127.	-12.5
	3	32.56	167.7	146.	-12.9
	4	66.15	340.7	262.	-23.1

ments, 18 reference points were chosen along the arch axis. As shown in Fig. 10, a miniature accelerometer sensitive only to radial acceleration(in-plane bending vibration) was affixed to the underside of the arch at an interior reference point. A small hammer fitted with a miniature accelerometer sensitive to accelerations in the direction of impact, was used to strike each of the reference points, excluding the points of support. The acceleration time histories measured at each strike were received by a signal analyzer(Model

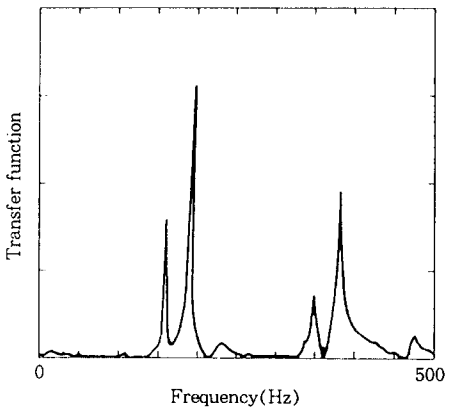

Fig. 11. Transfer function of acceleration for the clamped-hinged-clamped arch

SD390, Scientific Atlanta Corp.) and then processed by a microcomputer using a fast Fourier transform(FFT) analyzer. Using all of these data, the frequency dependent transfer function, defined as the ratio of the magnitude of the FFT of the arch acceleration to the magnitude of the FFT of the hammer acceleration.

Shown in Fig. 11 is the transfer function

of the clamped-hinged-clamped models. The frequencies for the major peaks of these plots are listed in Table 2. For the clamped-hinged-clamped arch, the four measured frequencies that occurred at first, second, third and fourth peak of the transfer function, Fig. 11, were 157, 194, 347 and 380 Hz, respectively. These four frequencies average about 9.7% less than the predicted values as shown in Table 2. Natural damping present in the experimental system but absent in the theoretical model contributes to the depression of the measured frequencies. The inevitable looseness of the end hinges and the difficulty in maintaining in-plane hammer strikes undoubtedly lead to out-of-plane vibrations, "noise" in the transfer function.

For the hinged-roller-hinged arch, the ideal end constraints were more difficult to achieve and this is reflected in the "crude" transfer function. As shown in Table 2, the measured frequencies are within 23% of the predicted values.

As discussed above, the experimental measures of frequencies for two laboratory-scale arch models serve to validate the theoretical results.

VII. Conclusions

By deriving the boundary conditions of intermediate supports of the multispan continuous arches, the numerical methods for calculating the free vibration, in-plane frequencies and mode shapes are found to be especially robust and reliable over a wide and practical range of arch parameters. In the numerical examples, the parabolic arches are considered and the hinged-roller-hinged and clamped-hinged-clamped support constraints are chosen. As the numerical results, the effects of rotary inertia and non-dimensional arch parameters on the natural frequencies are reported in tables and figures. Also experimental measures of frequencies for two laboratory-scale arch models serve to validate the theoretical results.

Acknowledgement

This paper was supported by NON-DIRECTED RESEARCH FUND, Korea Research Foundation, 1993. The authors appreciate for the financial support.

References

1. Austin, W.J. and Veletsos, A.S., 1973, "Free vibration of arches flexible in shear", Journal of Engineering Mechanics Division, ASCE, Vol.99(EM4), pp.735-753.
2. Borg, S.F. and Gennaro, J.J., 1959, Advanced Structural Analysis, New Jersey: Van Nostrand.
3. Carnahan, B., Luther, H.A. and Wikes, J. O., 1969, Applied Numerical Methods : John Wiley & Sons.
4. Ewins, D.J., 1985, Modal Testing: Theory and Practice, John Wiley, New York.
5. Ferziger, J.H., 1981, Numerical Methods for Engineering Application : John Wiley & Sons.
6. Henrych, J., 1981, The Dynamics of Arches and Frames : Elsevier Publishing Company.
7. Laura, P.A.A. and Maurizi, 1987, "Recent research in the vibration of arch-type structures", Shock and Vibration Digest, Vol.19, No.1, pp. 6-9.
8. Lee, B.K., Oh, S.J. and Mo, J.M., 1995 (accepted paper), "Approximate methods for natural frequencies and buckling loads of beam-columns with intermediate multiple elastic springs", Proceedings of 6th International Conference on Computing in Civil and Building Engineering, Berlin, Germany.
9. Lee, B.K. and Wilson, J.F., 1990, "Free vibrations of arches with variable curva-

ture", Journal of Sound Vibration, Vol. 36, No.1, pp.75-89.
10. Lee, B.K. and Wilson, J.F., submitted in 1994, "In-plane free vibrations of catenary arches with unsymmetric axes", Structural Engineering and Mechanics, An International Journal.
11. Perkins, N.C., 1990, "Planar vibration of an elastica arch: Theory and Experiment ", Journal of Vibration and Acoustics, Vol.112, pp.374-379.
12. Romanelli, E. and Laura, P.A.A., 1972, " Fundamental frequencies of non-circular, elastic, hinged arc", Journal of Sound and Vibration, Vol.24, No.1, pp.17-22.
13. Sakiyama, T., 1985, "Free vibration of arches with variable cross section and non-symmetric axis", Journal of Sound and Vibration, Vol.102, pp.448-452.
14. Veletsos, A.S., Austin, W.J. Pereira, C.A. L. and Wung, S.J., 1972, "Free in-plane vibration of circular arches", Journal of Engineering Mechanics Division, ASCE, Vol.98(EM2), pp.311-329.
15. Wang, T.M., 1972, "Lowest natural frequencies of elastic hinged arcs", Journal of the Acoustical Society of America, Vol.33, pp.1787-1790.
16. Wang, T.M. and Moore, J.A., 1973, " Lowest natural extensional frequency of clamped elliptic arcs", Journal of Sound and Vibration, Vol.30, pp.1-7.
17. Wilson, J.F, Lee, B.K. and Oh, S.J., 1994, "Free vibrations of arches with variable cross-section", Structural Engineering and Mechanics, An International Journal, Vol.2, No.3, pp.345-357.
18. Wolf, J.A., 1971, "Natural frequencies of circular arches", Journal of the Structural Division, ASCE, Vol.97(ST9), pp.2337 -2350.
19. Wung, S.J., 1967, Vibration of Hinged Circular Arches, Master's Thesis, Rice University, Houston, Texas, U.S.A.

(접수일자 : 1995년 2월 25일)